ESC European Society of Cardiology

European Heart Journal (2021) **42**, 3558–3571
doi:10.1093/eurheartj/ehab419

Extracellular vesicles from immortalized cardiosphere-derived cells attenuate arrhythmogenic cardiomyopathy in desmoglein-2 mutant mice

Yen-Nien Lin [1,2], Thassio Mesquita [1], Lizbeth Sanchez[1], Yin-Huei Chen[1,2], Weixin Liu [1], Chang Li[1], Russell Rogers [1], Yizhou Wang[3], Xinling Li [3], Di Wu [3], Rui Zhang[1], Ahmed Ibrahim [1], Eduardo Marbán[1], and Eugenio Cingolani[1]*

[1]Smidt Heart Institute, Cedars-Sinai Medical Center, 127 S. San Vicente Boulevard, Los Angeles, CA 90048, USA [2]Division of Cardiovascular Medicine, Department of Medicine, China Medical University and Hospital, 2, Yu-Der Road, North District, Taichung 40447, Taiwan; and [3]Genomics Core, Cedars-Sinai Medical Center, 8700 Beverly Blvd. Los Angeles, CA 90048, USA

Received 27 October 2020; revised 28 April 2021; editorial decision 8 June 2021; accepted 25 June 2021; online publish-ahead-of-print 29 July 2021

See page 3572 for the editorial comment on this article (doi:10.1093/eurheartj/ehab512)

Aims Arrhythmogenic cardiomyopathy (ACM) is characterized by progressive loss of cardiomyocytes, and fibrofatty tissue replacement. Extracellular vesicles (EVs) secreted by cardiosphere-derived cells, immortalized, and engineered to express high levels of β-catenin, exert anti-inflammatory, and anti-fibrotic effects. The aim of the current study was to assess efficacy of EVs in an ACM murine model.

Methods and results Four-week-old homozygous knock-in mutant desmoglein-2 ($Dsg2^{mt/mt}$) were randomized to receive weekly EVs or vehicle for 4 weeks. After 4 weeks, $DSG2^{mt/mt}$ mice receiving EVs showed improved biventricular function (left, $P < 0.0001$; right, $P = 0.0037$) and less left ventricular dilation ($P < 0.0179$). Electrocardiography revealed abbreviated QRS duration ($P = 0.0003$) and QTc interval ($P = 0.0006$) in EV-treated $DSG2^{mt/mt}$ mice. Further electrophysiology testing in the EV group showed decreased burden ($P = 0.0042$) and inducibility of ventricular arrhythmias ($P = 0.0037$). Optical mapping demonstrated accelerated repolarization ($P = 0.0290$) and faster conduction ($P = 0.0274$) in $Dsg2^{mt/mt}$ mice receiving EVs. $DSG2^{mt/mt}$ hearts exhibited reduced fibrosis, less cell death, and preserved connexin 43 expression after EV treatment. Hearts of $Dsg2^{mt/mt}$ mice expressed markedly increased levels of inflammatory cytokines that were, in part, attenuated by EV therapy. The pan-inflammatory transcription factor nuclear factor-κB (NF-κB), the inflammasome sensor NLRP3, and the macrophage marker CD68 were all reduced in EV-treated animals. Blocking EV hsa-miR-4488 *in vitro* and *in vivo* reactivates NF-κB and blunts the beneficial effects of EVs.

Conclusions Extracellular vesicle treatment improved cardiac function, reduced cardiac inflammation, and suppressed arrhythmogenesis in ACM. Further studies are needed prior to translating the present findings to human forms of this heterogenous disease.

* Corresponding author. Tel: +3102486679, Email: eugenio.cingolani@csmc.edu

Graphical Abstract

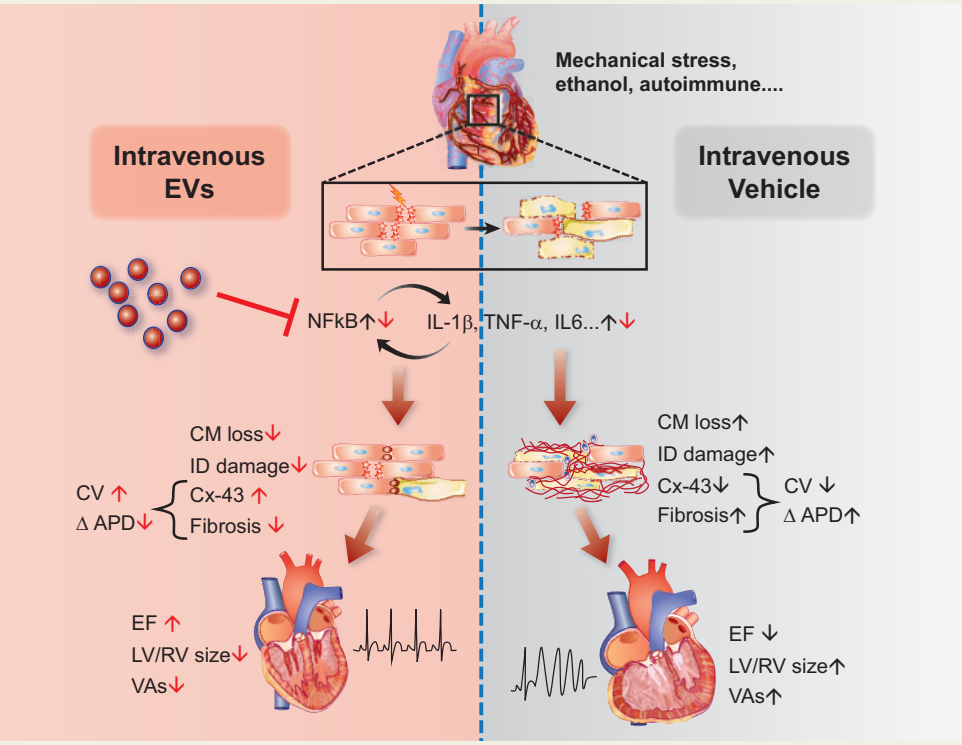

Salutary effects of extracellular vesicles (EVs) in arrhythmogenic cardiomyopathy resulting in improved ejection fraction (EF) and decreased ventricular arrhythmias (VAs). CM, Cardiomyocyte; IC, Intercalated disc; CV, Conduction velocity; APD, Action potential duration; LV/RV, Left Ventricle/Right Ventricle; Cx-43, Connexin-43.

Keywords Arrhythmogenic cardiomyopathy • Exosomes • Ventricular arrhythmia • Inflammation

Introduction

Arrhythmogenic cardiomyopathy (ACM) is an inherited heart disease affecting 1 in ~2500 individuals.[1] Defects in genes encoding desmosome proteins or their binding partners lead to malfunction of intercellular junctions in cardiac muscle, which normally absorb mechanical stress and favour membrane stability during cardiac contraction.[2–4] Desmosome dysfunction in cardiomyocytes produces membrane frailty, mitochondrial damage, disrupted cell signalling, and myocardial injury, which triggers progressive myocyte death, inflammatory activation, and ultimately fibrosis.[3] The fibrosis in turn leads to conduction slowing and re-entry circuits, favouring ventricular arrhythmias (VAs).[4] This complex pathophysiology results in heterogeneous clinical manifestations ranging from mild symptoms such as palpitations, to heart failure, and premature death.[5]

Pathophysiologically based interventions are notably lacking in the management of ACM patients, which focuses on activity restriction and generic anti-VA measures such as devices and catheter ablation.[4] Inflammation, however, does figure prominently in disease progression.[6–8] Patients with ACM have elevated circulating levels of pro-inflammatory cytokines [interleukin (IL)-1β, IL-6, and tumour necrosis factor-α (TNF-α)],[9] and compelling evidence supports the therapeutic benefits of blunting inflammatory signalling in ACM models.[7,10,11] Relevant interventions include inhibition of the complement factor C5a receptor (CD88),[10] blockade of glycogen synthase kinase-3β (GSK3β), an activator of nuclear factor-κB (NF-κB),[11,12] and Bay11-7082, a small molecule inhibitor of the inflammasome.[7] These findings, while not yet translated to the clinic, collectively suggest that immunomodulation merits further scrutiny as a treatment strategy in ACM.[8]

In an effort to address ACM more trenchantly, we investigated small extracellular vesicles (EVs), secreted by cardiosphere-derived cells (CDCs), as a therapeutic candidate. Cardiosphere-derived cells are stromal/progenitor cells with anti-inflammatory, immunomodulatory, anti-fibrotic, and cardiomyogenic properties mediated by EV secretion.[13] Although primary CDCs look generally promising in clinical trials for heart failure, Duchenne muscular dystrophy (DMD), and pulmonary hypertension,[13] variable potency has been a concern. We have recently shown that immortalized CDCs expressing high levels of β-catenin are therapeutically potent, and EVs from these CDCs consistently recapitulate the effects of CDCs in models of ischaemic injury.[14] Here, we tested the hypothesis that EVs are salutary in Dsg2 mutant ($Dsg2^{mt/mt}$) mice with ACM. Treatment with EVs

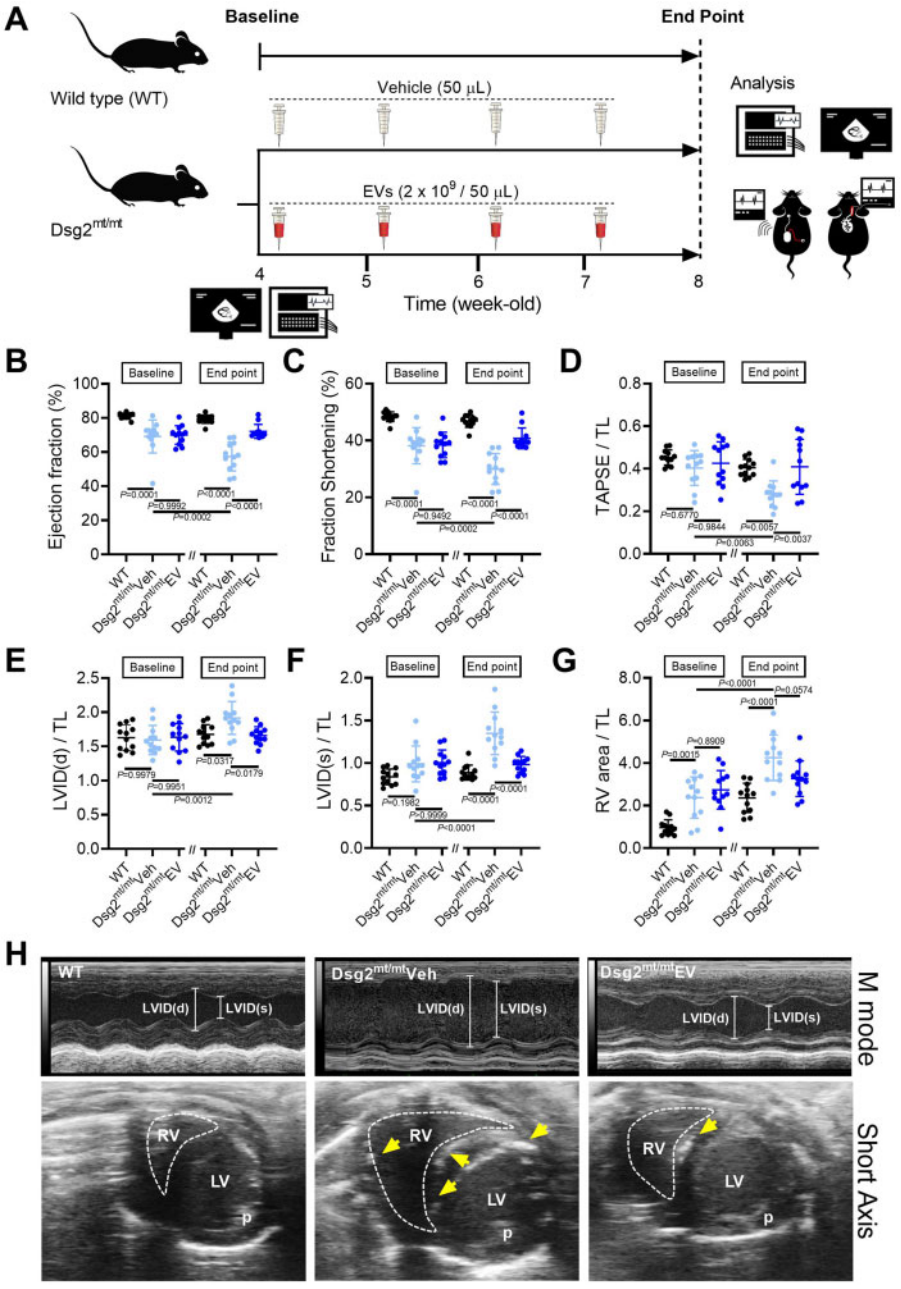

Figure 1 Intravenous extracellular vesicle injection improves myocardial injury and cardiac function in Dsg2$^{mt/mt}$ mice. (*A*) Experimental protocol. (*B–G*) Echo of wild type, vehicle-, and EV-treated Dsg2$^{mt/mt}$ mice. Data are mean ± SD; (n = 12 per group). *P*-values: one-way ANOVA with the Tukey's multiple-comparisons test. (*H*) Representative short-axis M-mode Echo from wild type, vehicle-, and EV-treated Dsg2$^{mt/mt}$ mice at 8 weeks of age. The yellow arrows indicate abnormal hyperechoic density. LV, left ventricle; LVIDd, left ventricular inner diastolic dimension; LVIDs, left ventricular inner systolic dimension; P, papillary muscle; RV, right ventricle; RVA, right ventricular area.

improved ventricular function and structure, attenuated fibrosis, and reduced arrhythmias.

Methods

A detailed description of all study methods including EV preparation, characterization, and biodistribution (Supplementary material online, *Figure S1*) is provided in the Supplementary material online.

Animal protocols

All animal studies were in full compliance with approved protocols of the Institutional Animal Care and Use Committee (IACUC # 7407). Four-week-old male or female mice (Dsg2$^{mt/mt}$ mice) with homozygous knock-in of a mutant form of *Dsg2*, and wild type (WT) age- and strain-matched animals were used in this study.[7,11] This *Dsg2* mutation entails loss of exon 4 and 5, which causes a frameshift and premature termination of translation. Mice were housed under pathogen-free conditions in a temperature-controlled room. Baseline electrocardiogram

(ECG) and echocardiogram were recorded prior to treatment with EVs or placebo. Extracellular vesicles (2.0×10^9) were suspended in 50 µL of Iscove's Modified Dulbecco's Medium (IMDM) and administered weekly via retro-orbital injections (to achieve intravenous delivery) in Dsg2$^{mt/mt}$ mice for four consecutive weeks. Vehicle-treated Dsg2$^{mt/mt}$ mice received an equal volume of IMDM weekly in the same manner for 4 weeks. Mice were reassessed for ECG, echocardiogram, and programmed electrical stimulation 4 weeks after therapy. Hearts were harvested for optical mapping experiments, and tissue was processed for histology and immunohistochemistry.

Echocardiography

Echocardiographic parameters were measured according to the American Society of Echocardiography guidelines.[15] Mice underwent two-dimensional transthoracic echocardiography at baseline (prior to treatment) and endpoint (after 4-week treatment). For details see Supplementary material online.

Electrocardiography

Electrocardiogram was recorded for 1 min during echocardiography with dual bio-amps (AD Instruments). Intervals (PR, QRS, QT, and RR) were measured and analysed using LabChart 7 software (AD Instruments) by a blinded trained observer. QTc interval was calculated as QT interval (ms) divided by the square root of the RR interval (ms) divided by 100.[16] The maximum slope-intercept method was used to define the end of the T wave.

Programmed electrical stimulation

Mice were anaesthetized with isoflurane inhalation with 2% isoflurane and core body temperature was kept at 36°C–38°C (rectal) with a heating lamp. Electrocardiogram was monitored during the procedure. A 1.1F octapolar electrophysiology catheter (Millar, EPR-800) was inserted via a jugular vein and advanced into the right atrium and ventricle. For details see Supplementary material online.

Statistical analysis

All results are expressed as the mean ± SD. Specific numbers and descriptions of statistical analyses are included in the legends for each figure and table. All statistical analyses were analysed with GraphPad Prism 8 Software. A *P*-value of <0.05 was considered statistically significant. Differences in measured variables were assessed with a two-tailed unpaired Student's *t*-test or Mann–Whitney test (if assumed non-Gaussian distribution). When comparing more than two groups, one-way analysis of variance (ANOVA) with Tukey's *post hoc* analysis to correct for multiple comparisons was applied. For comparisons of ventricular tachycardia (VT) inducibility, χ^2 test was used.

Results

Extracellular vesicles mitigate left and right ventricular dysfunction in arrhythmogenic cardiomyopathy

Based on the early increase of mortality in both sexes (Supplementary material online, *Figure S2A*) and the results of a pilot study (Supplementary material online, *Figure S2C–K*), treatment was initiated at 4 weeks of age and continued for 4 weeks (see *Figure 1A* for experimental overview). Relative to WT mice at baseline, Dsg2$^{mt/mt}$ mice display impaired left ventricular function (EF, 69.6 ± 7.7% vs. 81.1 ± 1.6%; $P = 0.0001$) and right ventricular dilatation (RVA/TL, 2.6 ± 0.9 vs. 1.0 ± 0.4; $P = 0.0001$) (*Figure 1B–G*). Follow-up echocardiography after 4 weeks of treatment revealed progressively worsening left ($P = 0.0002$) and right ventricular function ($P = 0.0063$) (*Figure 1B–D*) and chamber remodelling [left ventricle (LV), $P = 0.0012$; right ventricle (RV), $P < 0.0001$] (*Figure 1E–G*) in vehicle-injected Dsg2$^{mt/mt}$ mice. In contrast, those changes were prevented in EV-treated Dsg2$^{mt/mt}$ mice (*Figure 1B–G*, Supplementary material online, *Table S1*). Overall, EV–treated Dsg2$^{mt/mt}$ mice exhibited better biventricular function (LV, 72.2 ± 3.9% vs. 57.4 ± 8.0%; $P < 0.0001$; RV, 0.4 ± 0.1 vs. 0.3 ± 0.1; $P = 0.0037$) and less left ventricular dilatation (1.7 ± 0.1 vs. 1.9 ± 0.2; $P = 0.0179$) compared with controls. Although the right ventricular area was not statistically different in the EV and vehicle groups, echo images from vehicle mice showed numerous hyperechoic calcified lesions in the interventricular septum and right ventricular free wall; such lesions were infrequent after EV treatment (e.g., *Figure 1H*). In another Dsg2$^{mt/mt}$ cohort (Supplementary material online, *Figure S3A–H*), long-term EV treatment (for 8 weeks) prevented abnormal ventricular remodelling throughout the study. Interestingly, the cardiac protective effects persisted at least 4 weeks after EV therapy was completed.

Extracellular vesicles modify electrocardiographic abnormalities in arrhythmogenic cardiomyopathy

Arrhythmogenic cardiomyopathy is characterized by a high incidence of VAs, which can be fatal.[17] To investigate the effects of EVs on arrhythmic substrates, we examined ECG parameters at baseline and at study endpoint (*Figure 2A*). QTc interval was prolonged after vehicle injection (baseline vs. endpoint, 29.87 ± 6.2 ms vs. 37.97 ± 8.6 ms; $P = 0.0104$), but not in Dsg2$^{mt/mt}$ mice receiving EVs ($P = 0.9306$) (*Figure 2A and D*). At endpoint, vehicle-injected mice also displayed increased QRS and QTc intervals as compared with WT and EV-treated Dsg2$^{mt/mt}$ mice (*Figure 2B–D*). Additional ECG parameters, including heart rate and PR interval, were similar in the EV and vehicle groups (Supplementary material online, *Table S2* and *Figure S4A–C*).

Extracellular vesicles diminish arrhythmias in arrhythmogenic cardiomyopathy

The normalization of QRS and QTc by EVs indicates benefits on depolarization/conduction and repolarization, respectively, in Dsg2$^{mt/mt}$ mice, which may attenuate arrhythmogenesis. To characterize the burden and severity of VAs without impact from sedation, we used implanted ECG telemetry for ambulatory 24-h monitoring. Vehicle mice exhibited higher VA burden relative to EV mice (*Figure 2F*); indeed, the mean VA count was nine-fold higher in the vehicle group (71.1 ± 138.3/day vs. 8 ± 18.2/day; $P = 0.0042$) (*Figure 2G*). Representative ECG records in the vehicle group showed episodes of spontaneous VT (*Figure 2E*), while other events such as bigeminy, couplets, and isolated premature ventricular contractions (PVCs) were also seen. Importantly, other than isolated PVCs, no arrhythmias were observed in the EV group (*Figure 2E and H*).

To correlate provocative testing with the telemetry findings, we performed *in vivo* programmed electrical stimulation (PES) at study

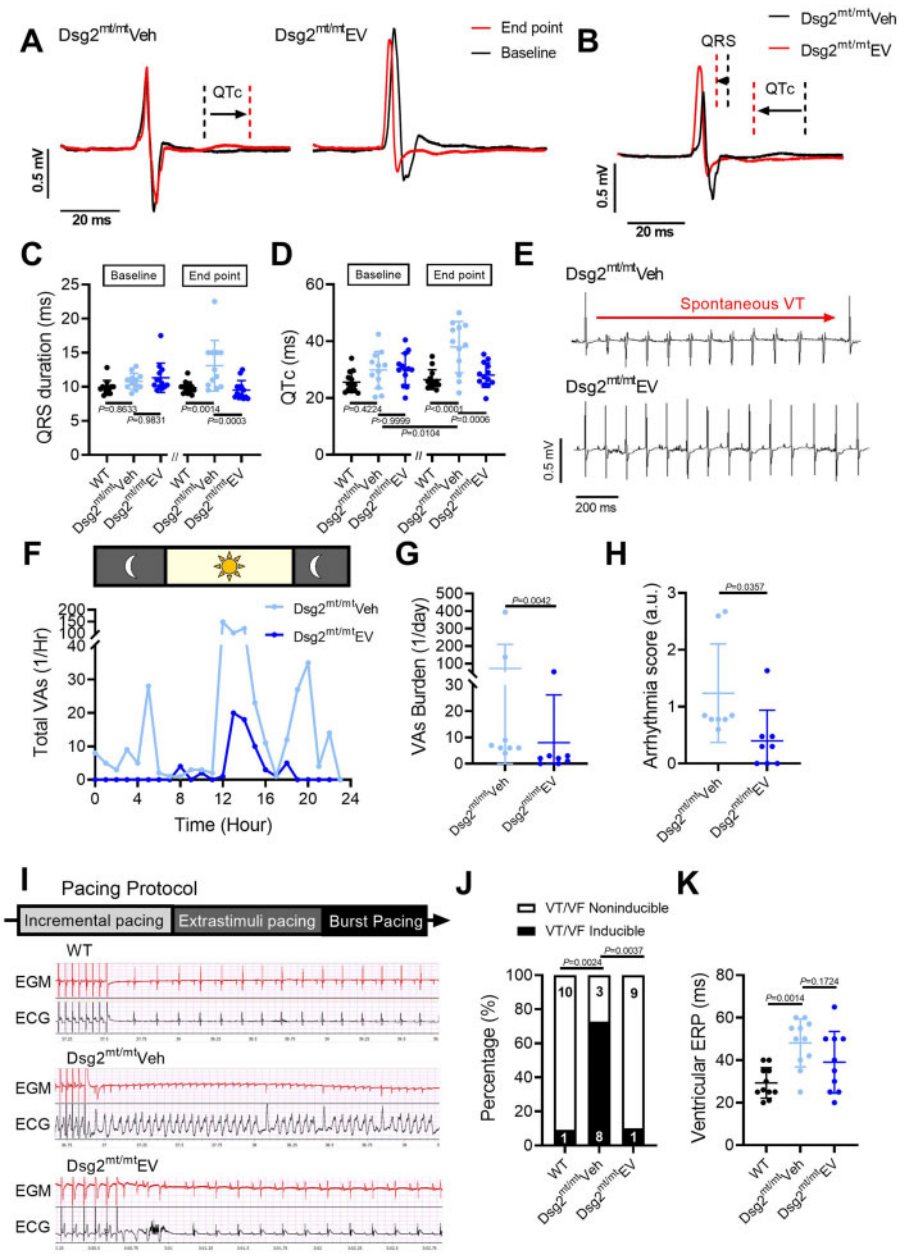

Figure 2 Extracellular vesicles improved ECG abnormalities and ventricular arrhythmias in Dsg2$^{mt/mt}$ mice. (*A*) Representative electrocardiogram tracings of Dsg2$^{mt/mt}$ mice received vehicle or extracellular vesicles (EVs) highlighting QRS and QT interval changes between baseline and endpoint. (*B*) Representative electrocardiogram tracings at the endpoint in Dsg2$^{mt/mt}$ mice comparing extracellular vesicle to vehicle group. (*C*, *D*) Electrocardiogram parameters of wild type, vehicle-, and extracellular vesicle-treated Dsg2$^{mt/mt}$ mice. Data are mean ± SD (*n* = wild type: 13; vehicle-injected: 12, extracellular vesicle-treated: 13; one mouse in vehicle group was dead during study period). *P*-values: one-way ANOVA with the Tukey's multiple-comparisons test. (*E*) Representative telemetry electrocardiogram tracings showing ventricular tachycardia (*top*) in vehicle-injected Dsg2$^{mt/mt}$ mice and a normal electrocardiogram tracing (*bottom*) in extracellular vesicle-treated Dsg2$^{mt/mt}$ mice. VT, ventricular tachycardia. (*F*) Twenty-four-hour run chart of total ventricular arrhythmias per hour. VAs, ventricular arrhythmias. (*G*) Quantification of ventricular arrhythmia burden. (*H*) Arrhythmia severity score in the vehicle group and the extracellular vesicle group (*n* = 8 per group). (*I*) Representative programmed electrical stimulation tracings and pacing protocol (*upper* panel, intracardiac electrogram; *lower* panel, surface electrocardiogram) in wild type (*top*), vehicle-injected (*middle*), and extracellular vesicle-treated (*bottom*) Dsg2$^{mt/mt}$ mice. EGM, electrogram. (*J*) Incidence of pacing-induced ventricular tachycardia (*n* = wild type: 11, vehicle-injected: 11; extracellular vesicle-treated: 10; one mouse in extracellular vesicle-treated group was dead during study period). (*K*) Quantification of ventricular effective refractory period (VERP). *P*-values: one-way ANOVA with the Tukey's multiple-comparisons test, Mann–Whitney test, and χ^2 test.

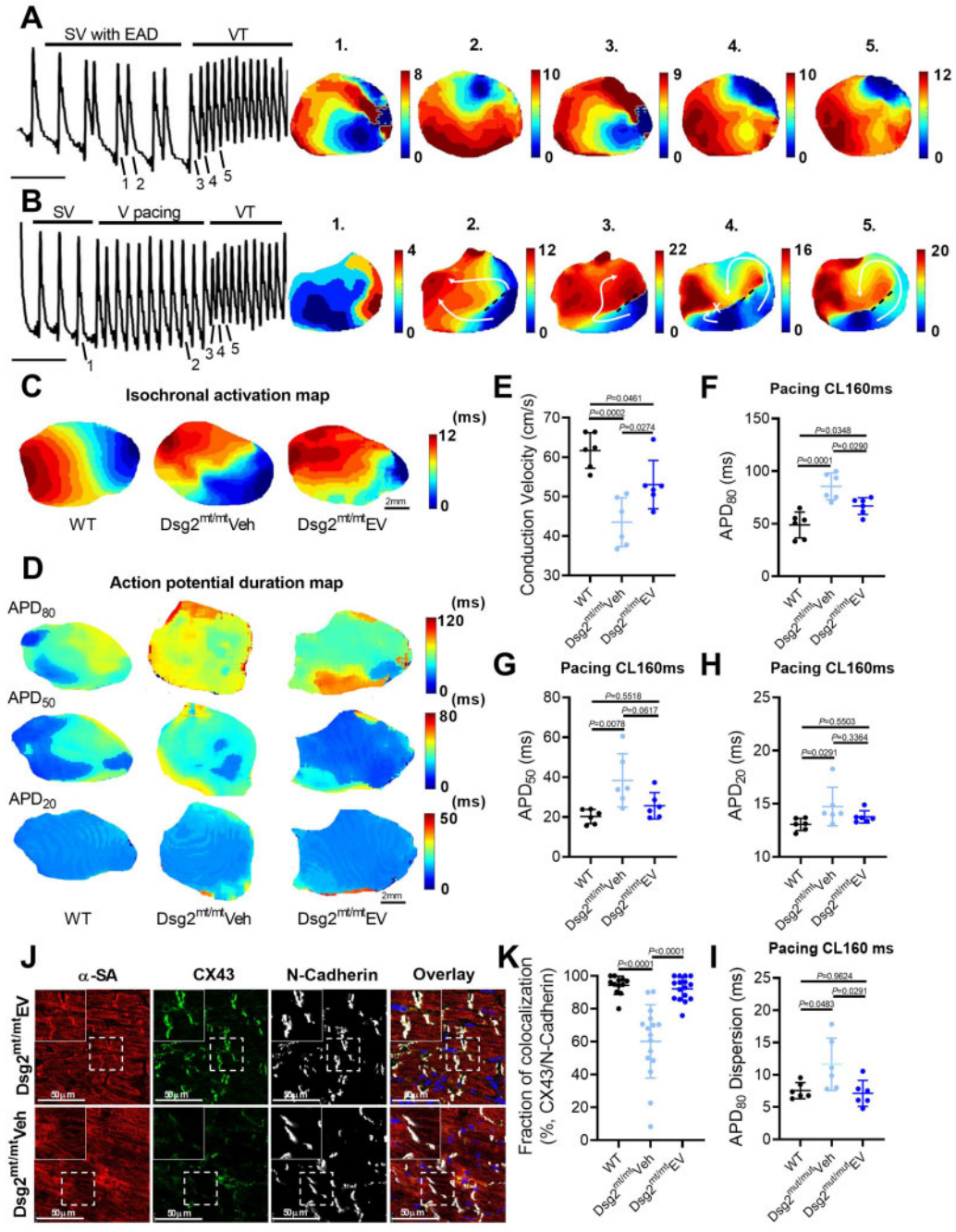

Figure 3 Mechanisms of ventricular arrhythmias in Dsg2$^{mt/mt}$ mice and electrical remodelling by extracellular vesicle therapy. (*A*, *B*) Representative images of optical action potential (*left*) and isochronal voltages map (*right*). EAD, early afterdepolarization; SV, sinus ventricular signal; VT, ventricular tachycardia. (*C*) Representative images of isochronal voltages map and conduction velocity (*E*). Representative images of action potential duration (APD) map at 160ms pacing cycle length (CL). (*F–H*) Quantification of action potential duration at 80% (APD_{80}), 50% (APD_{50}), and 20% (APD_{20}) repolarization and action potential duration dispersion (*I*) in 160 ms pacing conduction velocity ($n = 6$ per group). (*J*) Connexin 43 (CX43) immunostaining of the ventricle (*upper* panel: extracellular vesicle-treated Dsg2$^{mt/mt}$ mice; *lower* panel: vehicle-injected Dsg2$^{mt/mt}$ mice). (*K*) Quantification of Connexin 43 and N-cadherin colocalization. Data are mean ± SD ($n = 2–3$ sections per heart, 6 hearts per group). *P*-values: one-way ANOVA with the Tukey's multiple-comparisons test.

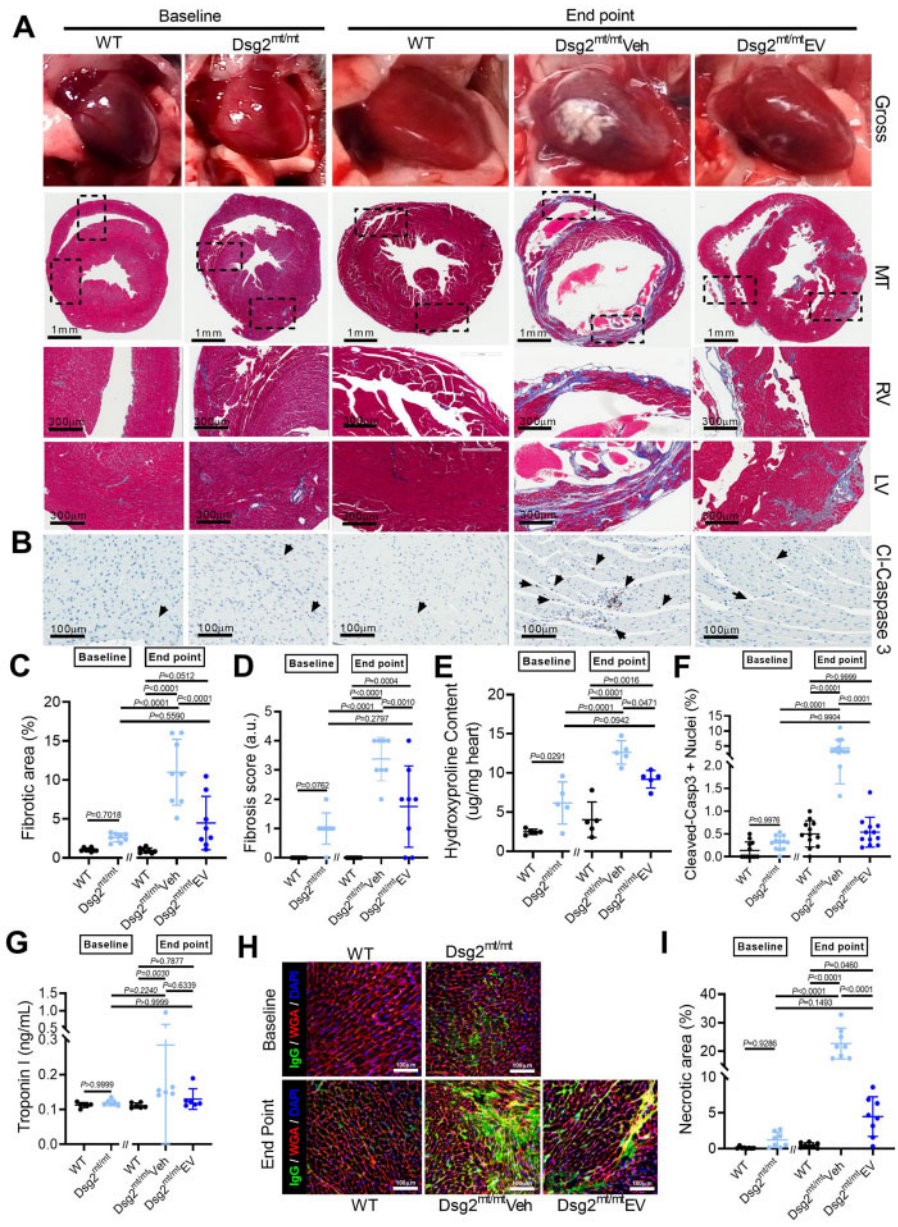

Figure 4 Extracellular vesicles ameliorate underlying cardiac fibrosis in Dsg2$^{mt/mt}$ mice. (*A*) Representative gross pathology (*top*) and Masson's trichrome-stained micrographs from wild type, Dsg2$^{mt/mt}$ hearts at baseline, and wild type, vehicle-, and extracellular vesicle (EV)-treated Dsg2$^{mt/mt}$ mouse hearts at the study endpoint. Scale bars for ventricle overview: 1 mm; for left and right ventricle: 300 µm. (*B*) Representative cleaved caspase 3 (cl-caspase 3) immunostaining of apoptotic cells for each group. Scale bars: 100 µm. (*C*) Pooled data from (*A*) revealed less fibrosis in extracellular vesicle-treated Dsg2$^{mt/mt}$ mouse hearts ($n = 8$ per group). (*D*) Quantification of fibrosis severity ($n = 8$ per group). (*E*) Quantification of cardiac hydroxyproline levels ($n = 5$ per group). (*F*) Pooled data from (*B*) revealed less apoptotic cells in extracellular vesicle-treated Dsg2$^{mt/mt}$ mouse hearts ($n = 2$ sections per heart, 6 hearts per group). (*G*) Necrosis of cardiomyocytes detected by troponin I release into the serum. (*H*) Representative images of IgG uptake in wild type, Dsg2$^{mt/mt}$ hearts at baseline, and wild type, vehicle-, and extracellular vesicle-treated Dsg2$^{mt/mt}$ mouse hearts at the study endpoint. Scale bars: 100 µm. (*I*) Quantification of the extent of cardiac myonecrosis ($n = 8$ per group). Data are mean ± SD. *P*-values: Kruskal–Wallis test with the Dunn's multiple-comparisons test, one-way ANOVA with the Tukey's multiple-comparisons test.

endpoint to assess VT inducibility (*Figure 2I*) . In the vehicle group, 72.7% of mice developed VT, whereas inducibility was similar, and low (10%), in WT and EV-treated Dsg2$^{mt/mt}$ mice (*Figure 2J*, Supplementary material online, *Figure S4D–F*). Consistent with changes in repolarization (QTc) seen on surface ECG, *in vivo* ventricular effective refractory period (VERP) measurement was significantly higher in vehicle-injected Dsg2$^{mt/mt}$ mice compared with WT mice (48.1 ± 11.3 ms vs. 29.3 ± 7.2 ms; $P = 0.0014$). Dsg2$^{mt/mt}$ mice

treated with EVs showed a trend, but not a significant decrease in VERP (38.9 ± 15.4 ms vs. 48.1 ± 11.3 ms; $P = 0.1724$) (*Figure 2K*). Consistently, the norepinephrine challenge test induced fewer PVCs in EV-treated mice compared with vehicle-injected controls (Supplementary material online, *Figure S4G–J*). Taken together, these observations indicate that EVs modify cardiac electrical remodelling in ACM, so as to suppress ventricular arrhythmic events.

Mechanisms of ventricular arrhythmias in arrhythmogenic cardiomyopathy

To better elucidate the mechanism(s) of VAs in ACM, we performed *ex vivo* optical mapping with a specific focus on how VTs are initiated in Dsg2$^{mt/mt}$ mice. *Figure 3A* shows optical action potentials under sinus rhythm with frequent ventricular early afterdepolarizations (EADs) preceding a spontaneous episode of VT in a Dsg2$^{mt/mt}$ heart. Isochronal activation maps revealed PVCs and VT originating from the same focal area (*Figure 3A*). Ventricular tachycardia could also be induced by PES at the apex (*Figure 3B*): isochronal activation maps show sinus ventricular activation with a region of conduction block (dotted line) that created dual-pathway physiology (white arrows in *Figure 3B2*). Subsequent electrical stimulation resulted in differences in conduction velocity and refractoriness between the two pathways (white arrows in *Figure 3B3-4*), which facilitated the VT re-entry circuit (white arrow in *Figure 3B5*). Thus, abnormal repolarization and conduction both contribute to arrhythmogenesis in this model: frequent EADs initiate focal VTs, while re-entrant VTs result from spatially distinct conduction velocities and refractoriness.

We next investigated the effects of EVs on the arrhythmogenic substrate in ACM. Ventricular APD and conduction velocity were measured using high-resolution optical mapping. *Figure 3C and E* shows that EVs significantly mitigated conduction slowing compared with vehicle (43.5 ± 6.2 cm/s vs. 53.1 ± 6.1 cm/s; $P = 0.0274$). Moreover, averaged APD_{80} (APD at 80% repolarization) was shortened (66.8 ± 7.9 ms vs. 85.4 ± 12.7 ms; $P = 0.0290$) (*Figure 3D and F–H*), and APD dispersion (7.1 ± 2.0 ms vs. 11.6 ± 4.0 ms; $P = 0.0291$) (measured as the standard deviation of APD_{80}) was decreased, in EV- compared with vehicle-injected mice (*Figure 3I*). The rise time of the optical action potential (a surrogate of sodium channel activity) was similar among experimental groups (3.6 ± 0.3 ms vs. 4.2 ± 0.7 ms vs. 4.0 ± 0.3 ms, $P = 0.1019$) (Supplementary material online, *Figure S4K*). In summary, optical mapping showed restoration of ventricular heterogeneity, both in terms of CV and APD, underlying the benefits of EVs on VAs in ACM.

Connexin 43 (Cx43) is the main gap junction type in the ventricular myocardium. Adverse remodelling of Cx43 is a feature of ACM, and explains, in part, impaired electrical conduction in this condition.[18] Accordingly, immunostaining revealed a significant down-regulation and redistribution of CX43 in the vehicle group, that was attenuated by EV treatment (92.1 ± 7.1% vs. 60.2 ± 22.3%; $P < 0.0001$) (*Figure 3J and K*). Extracellular vesicles also maintained plakoglobin expression at cell–cell junctions (Supplementary material online, *Figure S5*), indicating a relatively preserved intercalated disc structure.

Extracellular vesicles ameliorate underlying cardiac fibrosis in arrhythmogenic cardiomyopathy

Cardiac fibrous replacement, triggered by excessive myocyte death and inflammation, is a hallmark of ACM partially responsible for impaired electrical impulse propagation, and increased vulnerability for re-entrant arrhythmias. Hence, we investigated the effects of EVs on myocardial fibrosis. By gross pathology, WT and Dsg2$^{mt/mt}$ mice exhibited no whitish plaques at baseline, corresponding to minimal fibrosis by Masson trichrome staining (*Figure 4A, C, and D*). Compared with baseline histology, fibrosis increased significantly in 4-week vehicle-injected mice and was partially prevented by EV therapy (*Figure 4A, C, and D*, and Supplementary material online, *Figure S6*). The progression of fibrosis in each group was further confirmed by quantifying hydroxyproline content in each experimental group (*Figure 4E*). Taken together, these findings identify reduction in fibrosis as a contributor to improved cardiac function, and decreased arrhythmogenesis, in ACM after EV therapy. Moreover, the diminution of fibrosis in EV-treated Dsg2$^{mt/mt}$ mice is likely due to a reduction of fibrosis progression.

Extracellular vesicles attenuate cell death in arrhythmogenic cardiomyopathy

To study mechanisms underlying the reduction of fibrosis, we analysed cell death by immunostaining of cleaved caspase 3 (for apoptosis) and IgG (for necrosis) and quantified levels of serum troponin I (for necrosis). As shown in *Figure 4B and F*, at baseline, few apoptotic nuclei were seen in WT or Dsg2$^{mt/mt}$ mouse hearts. At the study endpoint, higher myocyte apoptosis was observed in vehicle-injected Dsg2$^{mt/mt}$ hearts compared with those in WT and EV-treated groups. Serum troponin I levels were low regardless of genotype or intervention at both baseline and endpoint, suggesting the necrotic process was insidious with periodic acute bursts (*Figure 4G*). Tissue immunostaining of cytoplasmic IgG revealed significant cell necrosis in Dsg2$^{mt/mt}$ hearts observed only at the endpoint (not baseline); EV treatment significantly reduced myonecrosis (*Figure 4H and I*). Together, these findings suggest cardiac fibrosis aligns with cell death.

Inflammation and extracellular vesicle therapy in arrhythmogenic cardiomyopathy

Inflammation has been recognized as a modifiable factor in the pathophysiology of ACM, influencing ventricular function, arrhythmias, and fibrosis.[6,7,10] Taking into consideration that EVs reduced cell death, we hypothesized a potential immunomodulatory response by EVs. To probe the effects of EVs on inflammation, we performed RNA sequencing (RNA-seq) in the three experimental groups. Relative to WT, heat maps revealed numerous changes of gene expression in vehicle-injected Dsg2$^{mt/mt}$ mice (*Figure 5A* and Supplementary material online, *Figure S7*), changes which were at least partially reverted towards WT levels by EV treatment (*Figure 5A* and Supplementary material online, *Figure S7*). In total, ~5700 disease-altered transcripts were 'corrected' by EVs (*Figure 5A*); among these are genes involved in fibrosis, heart failure, and inflammation (see *Figure 5B* for

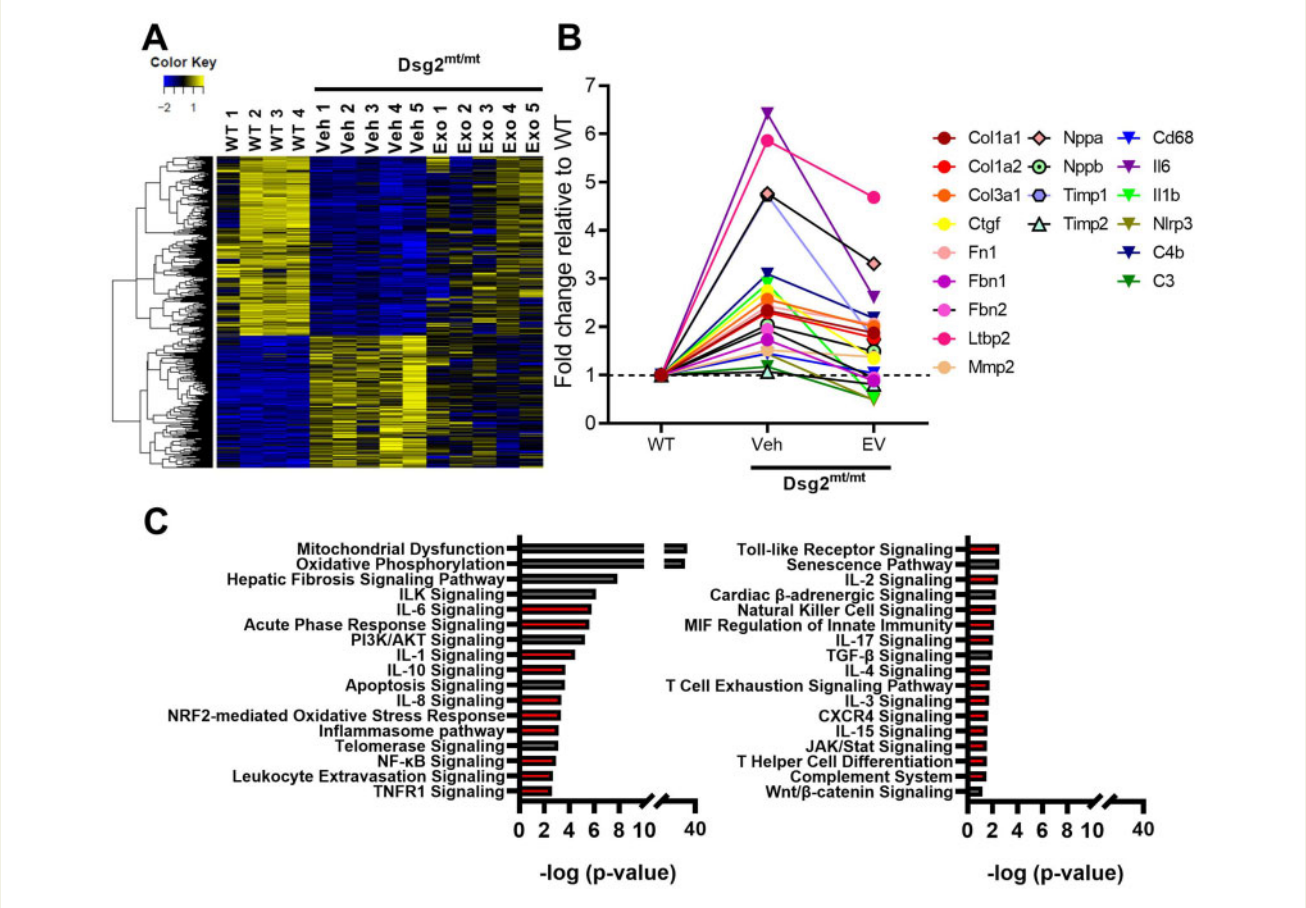

Figure 5 Transcriptomic analysis of therapeutic mechanisms associated with extracellular vesicles in Dsg2$^{mt/mt}$ mice. (*A*) Heat map showing transcripts that are up- or down-regulated in Dsg2$^{mt/mt}$ mouse hearts that were normalized partially or completely by extracellular vesicles (EV) treatment. (*B*) Selected genes involved in inflammation, fibrosis, or associated with heart failure that are rescued by extracellular vesicle treatment (abbreviations in Supplementary material online, *Table S3*). (*C*) Selected pathways up- or down-regulated in Dsg2$^{mt/mt}$ mice compared with wild type and modified by extracellular vesicle therapy. Red bars indicate inflammatory associated pathways.

examples). Ingenuity Pathway Analysis (IPA) identified many differentially expressed pathways related to inflammation and fibrosis (*Figure 5C*). The very notable changes in mitochondrial function and oxidative phosphorylation may reflect direct modification of these pathways, or simply changes in volume occupancy by scar (which, reciprocally, alter volume occupancy by living heart tissue, which is rich in mitochondria).[19] Additional experimentation will be required to distinguish between these possibilities.

Extracellular vesicles modulate the immune response in arrhythmogenic cardiomyopathy

Given the striking transcriptomic changes, we sought protein-level insight into the inflammatory response by quantifying inflammatory cytokines in the heart (*Figure 6A*). Compared to WT, vehicle-injected Dsg2$^{mt/mt}$ mice displayed increased levels of multiple pro-inflammatory cytokines, including IL-1α, IL-1β, IL-2, IL-4, IL-13, TNF-α, chemokine ligand-5 (RANTE), neutrophil chemoattractant LIX (CXCL-5), CXCL-1, B-cell chemoattractant (CXCL-13), monocyte chemoattractant protein-1 (MCP-1), and granulocyte-macrophage colony-stimulating factor (GM-CSF); EV treatment blunted most of these responses (*Figure 6B and C*).

Nuclear factor-κB, a master regulator of inflammatory gene expression, was up-regulated in vehicle-injected Dsg2$^{mt/mt}$ hearts (*Figure 6D*). Nuclear translocation of phosphorylated NF-κB, which primes NLRP3 and activates inflammasomes, induces the transcription of IL-1β and other pro-inflammatory factors.[20] In vehicle-injected Dsg2$^{mt/mt}$ hearts, activated NF-κB signalling was accompanied by the assembly of inflammasomes (NLRP3, ASC, Casp1-p20; *Figure 6D*). Extracellular vesicle treatment attenuated NF-κB phosphorylation and suppressed inflammasome formation (*Figure 6D*). Interleukin-1β level increased 10-fold in Dsg2$^{mt/mt}$ mice and was reduced towards WT levels by EV therapy, albeit non-significantly ($P = 0.0723$) (*Figure 6D*). Along with the changes in pro-inflammatory cytokines, macrophages in the heart—as gauged either by CD68 tissue levels (*Figure 6E*) or by immunohistochemistry (*Figure 6F*, Supplementary material online, *Figure S8F*)—followed the same pattern: up with vehicle, down with EVs.

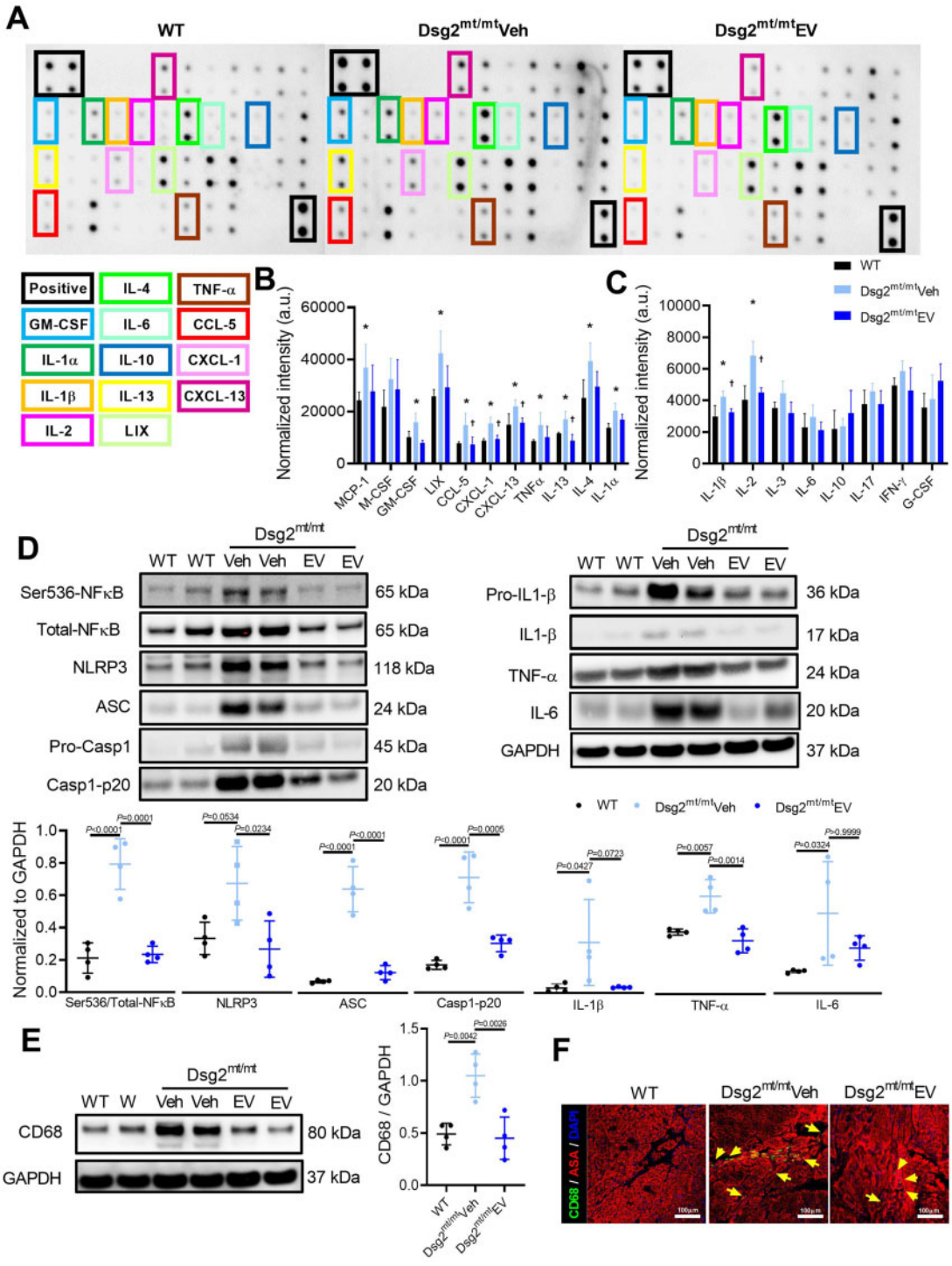

Figure 6 Modulation of immune response by extracellular vesicles in Dsg2$^{mt/mt}$ mice. (*A*) Representative cytokine array with quantification of relative intensity. (*B, C*) Cytokine levels in ventricular samples (n = 4 in each group). (*D*) Representative western blots (*top*) and quantified protein levels (*bottom*) of key immune regulators and cytokines of samples from wild type, vehicle-, extracellular vesicle-treated Dsg2$^{mt/mt}$ mice ventricles. (*E*) Representative western blots (*left*) and quantified protein levels (*right*) of macrophage lineage marker CD68 in wild type, vehicle-, extracellular vesicle-treated Dsg2$^{mt/mt}$ mouse ventricles. (*F*) Immunohistochemical staining for CD68 and α-sarcomeric actinin (ASA) in wild type, vehicle-, extracellular vesicle-treated Dsg2$^{mt/mt}$ mice. Scale bars: 100 μm. Data are mean ± SD. *P*-values: one-way ANOVA with the Tukey's multiple-comparisons test.

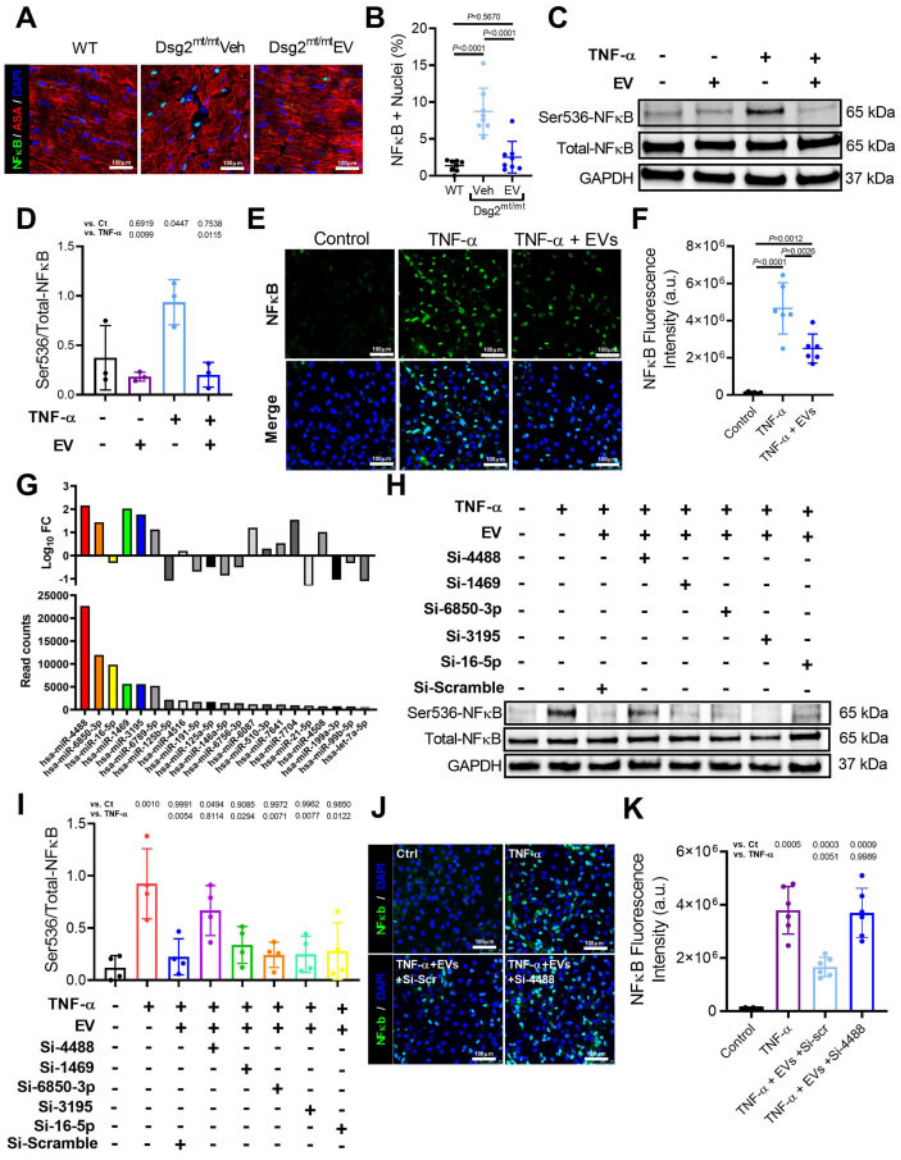

Figure 7 Reversal of nuclear factor-κB (NF-κB) activation by extracellular vesicles. (*A*) Immunohistochemical staining for nuclear factor-κB and α-sarcomeric actinin (ASA) in wild type, vehicle-injected, extracellular vesicle-treated Dsg2$^{mt/mt}$ mice. Scale bars: 100 μm. (*B*) Quantification of per cent of nuclei positive for nuclear factor-κB ($n = 8$ per group). (*C*) Representative western blot of neonatal rate ventricular myocyte (NRVM) protein extracts probed with antibodies to phosphorylated and total nuclear factor-κB, and GAPDH in control, TNF-α and extracellular vesicles groups. (*D*) Quantification of proteins level of phosphorylated and total NF-κB, and GAPDH ($n = 3$ per condition). (*E*) Representative immunohistochemical staining from control, NRVMs treated with TNF-α, and NRVMs treated with TNF-α and extracellular vesicles. (*F*) Quantification of NF-κB fluorescence intensity ($n = 6$ per condition). (*G*) Abundance and fold change of top 21 miRNAs identified in the extracellular vesicles. (*H*) Representative western blot of phosphorylated and total NF-κB, and GAPDH from TNF-α + extracellular vesicle-treated NRVMs transfected with top 5 miR inhibitors. (*I*) Quantification of proteins level of phosphorylated and total NF-κB, and GAPDH ($n = 4$ per condition). (*J*) Representative immunohistochemical staining from control, NRVMs treated with TNF-α, NRVMs treated with TNF-α, extracellular vesicles, and antagomir-scramble, and NRVMs treated with TNF-α, extracellular vesicles, and antagomiR-4488. (*K*) Quantification of NF-κB fluorescence intensity. ($n = 6$ per condition). Data are mean ± SD; *P*-values: one-way ANOVA with the Tukey's multiple-comparisons test.

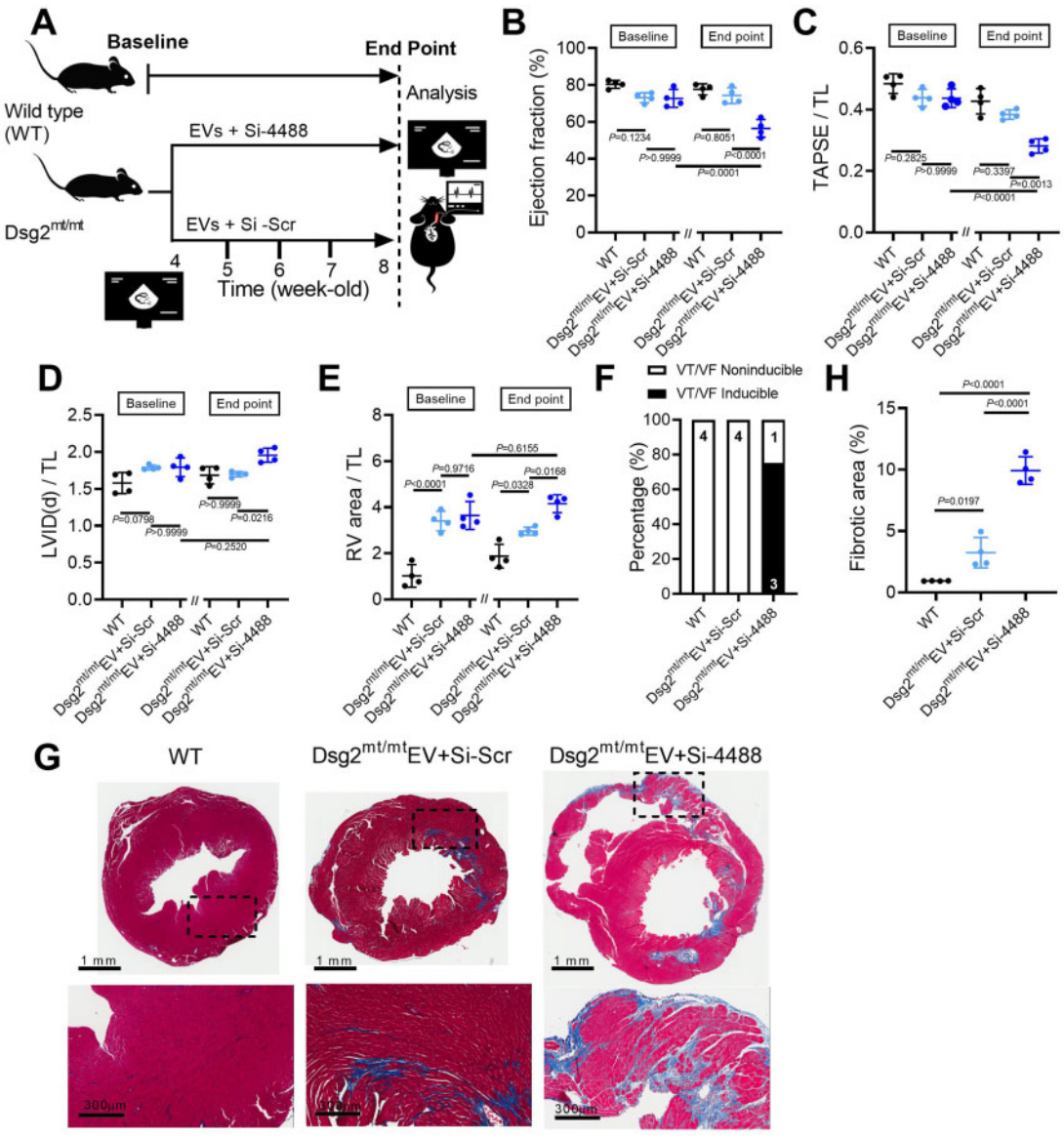

Figure 8 Antagomir-4488 blunts extracellular vesicle therapeutic effects in Dsg2$^{mt/mt}$ mice. (*A*) Experimental protocol. (*B–E*) Echo of wild type, extracellular vesicle + antagomir-scramble- (Si-scr), and extracellular vesicle + antagomir-4488-(Si-4488)-treated Dsg2$^{mt/mt}$ mice (n = 4 per group). (*F*) Incidence of pacing-induced ventricular tachycardia. (*G*) Representative Masson's trichrome–stained micrographs from wild type, extracellular vesicle + antagomir-scramble- (Si-scr), and extracellular vesicle + antagomir-4488-(Si-4488)-treated Dsg2$^{mt/mt}$ mice. Scale bars for ventricle overview: 1 mm; left ventricle: 300 μm. (*H*) Quantification of fibrotic area (n = 4 per group). Data are mean ± SD; *P*-values: one-way ANOVA with the Tukey's multiple-comparisons test.

Extracellular vesicles mitigate nuclear factor-κB activation via miR-4488 transfer to cardiomyocytes

Nuclear factor-κB activation can promote inflammation and myocyte death, while blocking NF-κB reverses the ACM phenotype.[7] To understand the role of this pathway in the salutary effects of EV therapy, we studied the effects of EVs on NF-κB on Dsg2$^{mt/mt}$ mice. After EV treatment, immunostaining from Dsg2$^{mt/mt}$ mice showed fewer cardiomyocytes positive for nuclear NF-κB compared with vehicle-injected or WT animals (*Figure 7A and B*). Consistently, using an *in vitro* neonatal rat ventricular myocyte (NRVM) model of TNF-α induced NF-κB activation, we showed decreased nuclear translocation of NF-κB after EV administration (*Figure 7C–F*).

Knowing EVs are associated with less NF-κB activation *in vitro* and *in vivo*, we then studied which EV components are responsible for these effects. RNA sequencing of both highly potent immortalized CDC-derived and primary CDC-derived EVs revealed >850 unique miRNAs in EVs isolated from both cell lines. The 21 most abundant miRNAs were used for downstream analysis (*Figure 7G*,

Supplementary material online, *Figure S8A–C*). Using NRVMs treated with either EVs or vehicle, co-transfection of antagomirs against the five most abundant miRNAs was performed. Transfection with antagomir-4488 increased NF-κB phosphorylation as TNF-α did (*Figure 7H and I*). Additionally, immunostaining confirmed that transfection of antagomir-4488 promoted nuclear translocation of NF-κB (*Figure 7J and K*). Collectively, these results suggest EVs mitigate NF-κB activation, in part, via miR-4488 transfer to cardiomyocytes.

Along with these findings, *in vitro* NRVM studies showed a significant reduction of TNF-α-induced apoptosis by pre-treatment with EVs, whereas antagomir-4488 blunted the anti-apoptotic effect of EVs (Supplementary material online, *Figure S8D* and *E*), indicating hsa-miR-4488 is important in reducing cell death.

Nuclear factor-κB activation causes cardiomyocyte death, and blocking hsa-miR-4488 has been reported to increase cell death[21]. Taken together, these findings support the hypothesis that the salutary effects of EVs in ACM can be, at least partially, explained by hsa-miR-4488 transfer to cardiomyocytes mediating a reduction in myocyte death.

Blocking hsa-miR-4488 blunts the beneficial effects of extracellular vesicles

We further examined whether antagomir-4488 can offset the therapeutic effects of EVs *in vivo*. Using the same study protocol (*Figure 8A*), antagomir-4488 was retro-orbitally injected to Dsg2$^{mt/mt}$ mice prior to each EV therapy. Follow-up echocardiography after 4 weeks of treatment revealed deterioration of left and right ventricular function (*Figure 8B and C*) and chamber enlargement (*Figure 8D and E*) in Dsg2$^{mt/mt}$ mice receiving combined treatment (antagomir-4488 and EVs) compared with EV alone. In line with the changes in cardiac function, Dsg2$^{mt/mt}$ mice treated with both antagomir-4488 and EVs displayed higher VT inducibility (*Figure 8F*) and larger extent of cardiac fibrosis compared with WT and animals treated with EVs alone (*Figure 8G and H*).

Protein profiling of extracellular vesicles

To further investigate the molecular processes that mediated the therapeutic effects of EVs, we have defined EV proteomic composition. Comparisons of proteins found in EVs from potent immortalized CDCs with primary CDCs revealed that proteins differentially expressed or unique to immortalized CDC EVs are chaperone proteins, metabolite interconversion enzymes, and cytoskeletal proteins (Supplementary material online, *Figure S9A–C* and *F*). Gene ontology analysis of biological processes identified these proteins important in cell growth and/or maintenance, energy pathways, metabolism, and signal transduction (Supplementary material online, *Figure S9D, E, G*, and *H*), which could facilitate myocyte recovery after injury[22,23].

β-catenin, highly expressed in potent immortalized CDCs, is essential in ACM pathogenesis when it is down-regulated[11]. Reduction and redistribution of Cx43 in Dsg2$^{mt/mt}$ mice are known to contribute to arrhythmogenesis[24]. To study the potential roles of β-catenin and Cx43 in the effects of EVs, we analysed the protein content from immortalized CDCs, EVs, and the transfer of these two proteins to target cells. Immunoblotting showed β-catenin and Cx43 to be quite low in EVs despite being high in CDCs (Supplementary material online, *Figure S10A*). Treating NRVMs with EVs did not increase β-catenin and Cx43 content (Supplementary material online, *Figure S10B* and *C*). Based on these findings, we conclude the EV contents of both β-catenin and Cx43 are very low, and EV therapy does not affect their expression in target cells.

Discussion

Arrhythmogenic cardiomyopathy is increasingly recognized as an inflammatory desmosomopathy accompanied by progressive myocyte death and fibrofatty infiltration.[6,7] The exact molecular mechanisms underlying this complex disease are not well-understood. Inflammation is an early and evolving feature of ACM and precedes any evident pathological feature of the disease.[7,25,26] Nevertheless, whether inflammation serves as the initial trigger or is a secondary response to cell death remains unclear. Regardless, inflammation can have a deleterious effect on the myocardium. Interventions targeted at complement receptor CD88,[10] and NF-κB,[7] ameliorate the disease phenotype *in vitro* and *in vivo*. Here, we provide further reason to implicate hyperinflammation as a major pathogenetic component of ACM. Repeated administration of EVs modulated the immune response, mitigated intercalated disc remodelling and fibrous infiltration, while improving cardiac function and blunting arrhythmias in ACM (*Graphical abstract*). The work here differs from previous studies of targeted therapies in using a cell-free therapeutic candidate derived from the secretome of stromal cells.

Collectively, these results highlight the critical role of NF-κB activation in ACM pathogenesis. Although the present findings are from a murine model, several lines of evidence support a role for NF-κB signalling in human ACM. Namely, induced pluripotent stem cell-derived cardiomyocytes from an ACM patient were found to have enhanced NF-κB signalling compared with healthy controls.[27] Moreover, inflammatory infiltration was more commonly seen in ACM patients who died suddenly.[28,29] Meanwhile, clinical interest in new NF-κB pathway inhibitors is growing.[30] Thus, the data are consistent with a role for NF-κB-mediated inflammation in human ACM, but the potential therapeutic value of NF-κB as a target in human ACM remains to be tested.

Interestingly, ACM and DMD share many histological and molecular/cellular pathogenic mechanisms.[31] Intramyocardial and intravenous injection of primary CDC-derived EVs reverses many features of DMD by blunting oxidative stress, mitochondrial dysfunction, inflammation, and fibrosis.[32,33] Two clinical trials of DMD have used primary CDCs, with promising benefits in both cardiac and skeletal muscle.[34,35] While the parent cells are viable therapeutic candidates, EVs transcend a number of limitations and disadvantages inherent to cell therapy. Here, we demonstrated that EVs from potent immortalized CDCs have similar pathophysiological consequences and regress ACM disease manifestations.

Even more than heart failure, VA is a defining feature of ACM. In the JUP^{2157del}2 ACM model, mice treated with the GSK-3 inhibitor (SB216763) exhibited lower PVC burden and shorter QRS duration.[11] Inactivation of NF-κB resulted in the elimination of late potentials in signal-averaged ECGs in Dsg2$^{mt/mt}$ mice.[7] However, little is known about the mechanisms whereby salutary interventions improve VAs and electrical remodelling in ACM. The present study provides mechanistic insights regarding the underlying causes of

arrhythmogenesis in ACM. We find that delayed repolarization and re-entry both contribute to VAs in ACM. Extracellular vesicles improved spontaneous and induced VAs by accelerating cardiac conduction, and by improving repolarization, with underlying reversal of Cx43 down-regulation, fibrosis, and inflammation.

Amelioration of the ACM phenotype by immune modulation has motivated the testing of additional therapeutic candidates, including a TNF-α inhibitor, pentoxifylline, and a monoclonal antibody against IL-1β, Canakinumab.[36] Our results raise the possibility that cell-derived cell-free therapies that modify immune signalling might be another mechanistically based therapy in ACM. Although $Dsg2^{mt/mt}$ mice recapitulate many of the human features of ACM (arrhythmogenicity and fibrosis), mouse hearts lack the fatty infiltrations seen in humans. In addition, these mice display an early and very aggressive phenotype (e.g. severe cardiomyopathy, QTc prolongation) that does not necessarily fit the broad spectrum of human disease presentation. Therefore, further pre-clinical and clinical studies are needed prior to translating the present findings to human forms of this heterogeneous disease.

Study limitations

Our study has several limitations. First of all, we have not established an unambiguous causal role for hyperinflammation in ACM pathogenesis, nor have we documented a correlation with inflammatory activity and disease severity. However, previous studies showed cytokines were positively correlated with myocardial injury and inversely correlated with cardiac function.[7] This suggests the salutary effects of EVs in ACM might be explained by the anti-inflammatory effects of CDC-derived EVs. Lastly, strenuous exercise is known to accelerate ACM progression and to increase arrhythmic risk, and as such, higher mortality rate has been documented in ACM mice receiving swimming training.[37] Future studies correlating animals' activity and response to EV therapy would give us important insights into this mechanistically based ACM therapy.

Supplementary material

Supplementary material is available at *European Heart Journal* online.

Acknowledgements

The authors thank Lisa Trahan for editorial assistance, and Daniel Judge (Medical University of South Carolina) for kindly providing the Dsg2 mutant mice that were re-derived at our facility.

Funding

Y.-N.L. was supported by China Medical University and Hospital (CMU107-N-05). General lab support was provided by grants from the National Institutes of Health (R01 HL124074, R01 HL135866, and R01 HL147570), the Peer-Reviewed Medical Research Program of the U.S. Department of Defense (PR150620), and the Cedars-Sinai Board of Governors. E.M. holds the Mark S. Siegel Family Foundation Distinguished Chair of the Cedars-Sinai Medical Center.

Conflict of interest: E.M. owns founder's equity in Capricor Therapeutics. The other authors have nothing to disclose.

References

1. Basso C, Corrado D, Marcus FI, Nava A, Thiene G. Arrhythmogenic right ventricular cardiomyopathy. *Lancet* 2009;**373**:1289—1300.
2. Towbin JA, McKenna WJ, Abrams DJ, Ackerman MJ, Calkins H, Darrieux FCC, Daubert JP, de Chillou C, DePasquale EC, Desai MY, Estes NAM, Hua W, Indik JH, Ingles J, James CA, John RM, Judge DP, Keegan R, Krahn AD, Link MS, Marcus FI, McLeod CJ, Mestroni L, Priori SG, Saffitz JE, Sanatani S, Shimizu W, van Tintelen JP, Wilde AAM, Zareba W. 2019 HRS expert consensus statement on evaluation, risk stratification, and management of arrhythmogenic cardiomyopathy. *Heart Rhythm Elsevier* 2019;**16**:e301—e372.
3. Austin KM, Trembley MA, Chandler SF, Sanders SP, Saffitz JE, Abrams DJ, Pu WT. Molecular mechanisms of arrhythmogenic cardiomyopathy. *Nat Rev Cardiol* 2019;**16**:519—537.
4. Corrado D, Basso C, Judge DP. Arrhythmogenic cardiomyopathy. *Circ Res* 2017;**121**:784—802.
5. Mattesi G, Zorzi A, Corrado D, Cipriani A. Natural history of arrhythmogenic cardiomyopathy. *J Clin Med* 2020;**9**:878.
6. Lubos NG, S van der Gerçek M, Kant S, Leube RE, Krusche CA. Inflammation shapes pathogenesis of murine arrhythmogenic cardiomyopathy. *Basic Res Cardiol* 2020;**115**:42.
7. Chelko SP, Asimaki A, Lowenthal J, Bueno-Beti C, Bedja D, Scalco A, Amat-Alarcon N, Andersen P, Judge DP, Tung L, Saffitz JE. Therapeutic modulation of the immune response in arrhythmogenic cardiomyopathy. *Circulation* 2019;**140**:1491—1505.
8. Caforio ALP, Re F, Avella A, Marcolongo R, Baratta P, Seguso M, Gallo N, Plebani M, Izquierdo-Bajo A, Cheng C-Y, Syrris P, Elliott PM, Amati G. D, Thiene G, Basso C, Gregori D, Iliceto S, Zachara E. Evidence from family studies for autoimmunity in arrhythmogenic right ventricular cardiomyopathy: associations of circulating anti-heart and anti-intercalated disk autoantibodies with disease severity and family history. *Circulation* 2020;**141**:1238—1248.
9. Asimaki A, Tandri H, Duffy ER, Winterfield JR, Mackey-Bojack S, Picken MM, Cooper LT, Wilber DJ, Marcus FI, Basso C, Thiene G, Tsatsopoulou A, Protonotarios N, Stevenson WG, McKenna WJ, Gautam S, Remick DG, Calkins H, Saffitz JE. Altered desmosomal proteins in granulomatous myocarditis and potential pathogenic links to arrhythmogenic right ventricular cardiomyopathy. *Circ Arrhythm Electrophysiol* 2011;**4**:743—752.
10. Mavroidis M, Davos CH, Psarras S, Varela A, C Athanasiadis N, Katsimpoulas M, Kostavasili I, Maasch C, Vater A, van Tintelen JP, Capetanaki Y. Complement system modulation as a target for treatment of arrhythmogenic cardiomyopathy. *Basic Res Cardiol* 2015;**110**:27.
11. Chelko SP, Asimaki A, Andersen P, Bedja D, Amat-Alarcon N, DeMazumder D, Jasti R, MacRae CA, Leber R, Kleber AG, Saffitz JE, Judge DP. Central role for GSK3β in the pathogenesis of arrhythmogenic cardiomyopathy. *JCI Insight* 2016;**1**:e85923.
12. Padrón-Barthe L, Villalba-Orero M, Gómez-Salinero JM, Domínguez F, Román M, Larrasa-Alonso J, Ortiz-Sánchez P, Martínez F, López-Olañeta M, Bonzón-Kulichenko E, Vázquez J, Martí-Gómez C, Santiago DJ, Prados B, Giovinazzo G, Gómez-Gaviro MV, Priori S, Garcia-Pavia P, Lara-Pezzi E. Severe cardiac dysfunction and death caused by arrhythmogenic right ventricular cardiomyopathy type 5 are improved by inhibition of glycogen synthase kinase-3β. *Circulation* 2019;**140**:1188—1204.
13. Marbán E. A mechanistic roadmap for the clinical application of cardiac cell therapies. *Nat Biomed Eng* 2018;**2**:353—361.
14. Ibrahim AGE, Li C, Rogers R, Fournier M, Li L, Vaturi SD, Antes T, Sanchez L, Akhmerov A, Moseley JJ, Tobin B, Rodriguez-Borlado L, Smith RR, Marbán L, Marbán E. Augmenting canonical Wnt signalling in therapeutically inert cells converts them into therapeutically potent exosome factories. *Nat Biomed Eng* 2019;**3**:695—705.
15. Syed F, Diwan A, Hahn HS. Murine echocardiography: a practical approach for phenotyping genetically manipulated and surgically modeled mice. *J Am Soc Echocardiogr* 2005;**18**:982—990.
16. Mitchell GF, Jeron A, Koren G. Measurement of heart rate and Q-T interval in the conscious mouse. *Am J Physiol* 1998;**274**:H747—H751.
17. Costa S, Cerrone M, Saguner AM, Brunckhorst C, Delmar M, Duru F. Arrhythmogenic cardiomyopathy: an in-depth look at molecular mechanisms and clinical correlates. *Trends Cardiovasc Med* 2020;S1050-1738(20)30103-1.
18. Noorman M, Hakim S, Kessler E, Groeneweg JA, Cox MGPJ, Asimaki A, van Rijen HVM, van Stuijvenberg L, Chkourko H, van der Heyden MAG, Vos MA, de Jonge N, van der Smagt JJ, Dooijes D, Vink A, de Weger RA, Varro A, de Bakker JMT, Saffitz JE, Hund TJ, Mohler PJ, Delmar M, Hauer RNW, van Veen TAB. Remodeling of the cardiac sodium channel, connexin43, and plakoglobin at the intercalated disk in patients with arrhythmogenic cardiomyopathy. *Heart Rhythm* 2013;**10**:412—419.
19. Park S-Y, Gifford JR, Andtbacka RHI, Trinity JD, Hyngstrom JR, Garten RS, Diakos NA, Ives SJ, Dela F, Larsen S, Drakos S, Richardson RS. Cardiac, skeletal,

and smooth muscle mitochondrial respiration: are all mitochondria created equal? *Am J Physiol Heart Circ Physiol* 2014;**307**:H346—H352.
20. Lamkanfi M, Dixit VM. Mechanisms and functions of inflammasomes. *Cell* 2014; **157**:1013—1022.
21. Fang SY, Huang CW, Huang TC, Yadav A, Chiu JJ, Wu CC. Reduction in microRNA-4488 expression induces NFκB translocation in venous endothelial cells under arterial flow. *Cardiovasc Drugs Ther* 2021;**35**:61—71.
22. Nair SP, Sharma RK. Heat shock proteins and their expression in primary murine cardiac cell populations during ischemia and reperfusion. *Mol Cell Biochem* 2020; **464**:21—26.
23. Chelko SP, Keceli G, Carpi A, Doti N, Agrimi J, Asimaki A, Beti CB, Miyamoto M, Amat-Codina N, Bedja D, Wei A-C, Murray B, Tichnell C, Kwon C, Calkins H, James CA, O'Rourke B, Halushka MK, Melloni E, Saffitz JE, Judge DP, Ruvo M, Kitsis RN, Andersen P, Lisa FD, Paolocci N. Exercise triggers CAPN1-mediated AIF truncation, inducing myocyte cell death in arrhythmogenic cardiomyopathy. *Sci Transl Med* 2021;**13**:eabf0891.
24. Poelzing S, Rosenbaum DS. Altered connexin43 expression produces arrhythmia substrate in heart failure. *Am J Physiol Heart Circ Physiol* 2004;**287**: H1762—H1770.
25. Psarras S, Mavroidis M, Sanoudou D, Davos CH, Xanthou G, Varela AE, Panoutsakopoulou V, Capetanaki Y. Regulation of adverse remodelling by osteopontin in a genetic heart failure model. *Eur Heart J* 2012;**33**:1954—1963.
26. Pilichou K, Remme CA, Basso C, Campian ME, Rizzo S, Barnett P, Scicluna BP, Bauce B, van den Hoff MJB, de Bakker JMT, Tan HL, Valente M, Nava A, Wilde AAM, Moorman AFM, Thiene G, Bezzina CR. Myocyte necrosis underlies progressive myocardial dystrophy in mouse dsg2-related arrhythmogenic right ventricular cardiomyopathy. *J Exp Med* 2009;**206**:1787—1802.
27. Asimaki A, Protonotarios A, James CA, Chelko SP, Tichnell C, Murray B, Tsatsopoulou A, Anastasakis A, Te Riele, A, Kléber AG, Judge DP, Calkins H, Saffitz JE. Characterizing the molecular pathology of arrhythmogenic cardiomyopathy in patient buccal mucosa cells. *Circ Arrhythm Electrophysiol* 2016;**9**:e003688.
28. Fontaine G, Fontaliran F, Andrade FR, Velasquez E, Tonet J, Jouven X, Fujioka Y, Frank R. The arrhythmogenic right ventricle. Dysplasia versus cardiomyopathy. *Heart Vessels* 1995;**10**:227—235.
29. Corrado D, Basso C, Thiene G, McKenna WJ, Davies MJ, Fontaliran F, Nava A, Silvestri F, Blomstrom-Lundqvist C, Wlodarska EK, Fontaine G, Camerini F. Spectrum of clinicopathologic manifestations of arrhythmogenic right ventricular cardiomyopathy/dysplasia: a multicenter study. *J Am Coll Cardiol* 1997;**30**: 1512—1520.
30. Ramadass V, Vaiyapuri T, Tergaonkar V. Small molecule NF-κB pathway inhibitors in clinic. *Int J Mol Sci* 2020;**21**:5164. doi: 10.3390/ijms21145164.
31. Gao S, Chen SN, Di Nardo C, Lombardi R. Arrhythmogenic cardiomyopathy and skeletal muscle dystrophies: shared histopathological features and pathogenic mechanisms. *Front Physiol* 2020;**11**:834.
32. Rogers RG, Fournier M, Sanchez L, Ibrahim AG, Aminzadeh MA, Lewis MI, Marbán E. Disease-modifying bioactivity of intravenous cardiosphere-derived cells and exosomes in mdx mice. *JCI Insight* 2019;**4**:e125754.
33. Aminzadeh MA, Rogers RG, Fournier M, Tobin RE, Guan X, Childers MK, Andres AM, Taylor DJ, Ibrahim A, Ding X, Torrente A, Goldhaber JM, Lewis M, Gottlieb RA, Victor RA, Marbán E. Exosome-mediated benefits of cell therapy in mouse and human models of Duchenne muscular dystrophy. *Stem Cell Reports* 2018;**10**:942—955.
34. Taylor M, Jefferies J, Byrne B, Lima J, Ambale-Venkatesh B, Ostovaneh MR, Makkar R, Goldstein B, Smith RR, Fudge J, Malliaras K, Fedor B, Rudy J, Pogoda JM, Marbán L, Ascheim DD, Marbán E, Victor RG. Cardiac and skeletal muscle effects in the randomized HOPE-Duchenne trial. *Neurology* 2019;**92**: e866—e878.
35. Marban L, Rogy S, McDonald C, Eagle M, Finkel R, Tian C, Taylor M, Janas J, Harmelink M, Varadhachary A, Hor K, Mayer OH, Furlong P. HOPE-2 one-year results show clinically relevant improvements in upper limb and cardiac function in patients with later stage Duchenne Muscular Dystrophy (abstr). *Neuromuscul Disord* 2020;**30**:S168—S169.
36. van der Voorn SM, Te Riele ASJM, Basso C, Calkins H, Remme CA, van Veen TAB. Arrhythmogenic cardiomyopathy: pathogenesis, pro-arrhythmic remodelling, and novel approaches for risk stratification and therapy. *Cardiovasc Res* 2020; **116**:1571—1584.
37. Prior D, La Gerche A. Exercise and arrhythmogenic right ventricular cardiomyopathy. *Heart Lung Circ* 2020;**29**:547—555.